Journal of Medicinal Chemistry

Brief Article

Small molecule antagonists of the interaction between the histone deacetylase 6 zinc-finger domain and ubiquitin

Rachel J. Harding, Renato Ferreira de Freitas, Patrick Michael Collins, Ivan Franzoni, Mani Ravichandran, Hui Ouyang, Kevin A. Juarez-Ornelas, Mark Lautens, Matthieu Schapira, Frank von Delft, Vijayaratnam Santhakumar, and Cheryl H. Arrowsmith

J. Med. Chem., **Just Accepted Manuscript** • Publication Date (Web): 11 Oct 2017

Just Accepted

ACS Publications

Journal of Medicinal Chemistry is published by the American Chemical Society. 1155 Sixteenth Street N.W., Washington, DC 20036

Small molecule antagonists of the interaction between the histone deacetylase 6 zinc-finger domain and ubiquitin

Rachel J. Harding†, Renato Ferreira de Freitas†, Patrick Collins‡, Ivan Franzoni¶, Mani Ravichandran†, Hui Ouyangᵠ, Kevin A. Juarez-Ornelas¶, Mark Lautens¶, Matthieu Schapira†#, Frank von Delft‡§, Vjayaratnam Santhakumar†, Cheryl H. Arrowsmith†*

†Structural Genomics Consortium, University of Toronto, MaRS South Tower, Suite 700, 101 College Street, Toronto, ON M5G 1L7, Canada, ‡Diamond Light Source Ltd, Harwell Science and Innovation Campus, Didcot OX11 0QX, U.K., ¶Department of Chemistry, Davenport Chemical Laboratories, 80 St. George St., University of Toronto, Toronto, Ontario, M5S 3H6 Canada, ᵠGrandPharma, Wuhan City Plaza, 23rd Floor, 160 Qiaokou Rd, Wuhan, Hubei, China, #Department of Pharmacology and Toxicology, University of Toronto, Toronto, ON M5S 1A8, Canada, §Structural Genomics Consortium, University of Oxford, Roosevelt Drive, Oxford OX11 9HP, U.K.

ABSTRACT: Inhibitors of HDAC6 have attractive potential in numerous cancers. HDAC6 inhibitors to date target the catalytic domains, but targeting the unique zinc-finger ubiquitin-binding domain (Zf-UBD) of HDAC6 may be an attractive alternative strategy. We developed X-ray crystallography and biophysical assays to identify and characterize small molecules capable of binding to the Zf-UBD and competing with ubiquitin binding. Our results revealed two adjacent ligand-able pockets of HDAC6 Zf-UBD and the first functional ligands for this domain.

INTRODUCTION Histone deacetylases (HDACs) comprise a family of 18 enzymes with diverse roles in mammalian cell homeostasis[1,2]. HDAC6 is distinct from other zinc-dependent catalytic enzymes in this class, with unique features including two functional catalytic domains and a zinc-finger ubiquitin binding domain (Zf-UBD) spanning resides 1109-1215[3–6]. Localized to the cytosol, HDAC6 has diverse roles in the function of the cytoskeleton[7,8], cell migration[9], cell reprogramming and pluripotency[10,11] and is implicated in numerous pathologies including cancer[12], neurodegeneration[13,14] and viral infection[15,16]. HDAC6 can deacetylate many non-histone proteins including α-tubulin[8,15,17], HSP90[18] and cortactin[19]. HDAC6 knockout mouse studies show elevated acetylation levels in more than 100 proteins in the liver[20,21] suggesting that HDAC6 may deacetylate a wide range of substrates *in vivo,* reflecting its diverse cellular roles. A deep cavity in the Zf-UBD of HDAC6 binds the C-terminal RLRGG motif of free ubiquitin as well as C-terminally unanchored polyubiquitin moieties with high affinity[4,5,22], leading to its activation[23]. This promotes the autophagic clearance of ubiquitinated protein aggregates in the cell by gathering and loading them on dynein for aggresome formation and degradation[24]. The Zf-UBD is also involved in the recruitment of HDAC6 to influenza viral fusion sites and subsequent infection[25,26]. Inhibitors of this domain could represent a novel mechanism to interrupt the viral life cycle.

Numerous specific and potent inhibitors of HDAC6 catalytic domains have been developed[27–30] which prevent deacetylation of tubulin, a modification required for transport of misfolded proteins along microtubules to the aggresome[31]. Used in combination with proteasome inhibitors, HDAC6 catalytic inhibitors can promote apoptosis in a number of different hematological malignancies including multiple myeloma and lymphoma[32–36]. Challenges related to tedious chemical synthesis[37,38], low bioavailability[39] and cytotoxicity for hydroxamate-based compounds[40] have been reported for some HDAC6 inhibitors. Targeting the recognition of protein aggregates by the Zf-UBD[41] rather than their loading on microtubules as catalytic inhibitors do, could be an alternative mechanism to antagonize aggresome degradation.

In order to identify novel antagonists and ligands of the HDAC6 Zf-UBD, we developed and optimized three different biophysical binding assays as well as a crystallographic method for screening ligands for this domain. We then performed a high throughput screen of fragments using X-ray crystallography as well as a virtual screen using the crystal structure bound to the ubiquitin C-terminal peptide. We initially identified four small molecule ligands of HDAC6 Zf-UBD and characterized them by surface plasmon resonance (SPR), fluorescence polarization (FP) peptide displacement assay and isothermal titration calorimetry (ITC). Preliminary structure–activity relationship (SAR) studies found compounds of improved potency, able to displace a FITC-labelled C-terminal ubiquitin RLRGG peptide, as well as a compound which links the two ligand-able pockets

Table 1. Initial ligands identified by virtual and X-ray crystallography fragment screen.

Ligands	**1**	**2**	**3**	**4**
Cocrystal PDB codes	5KH9	5B8D	5KH3	5KH7
Structure	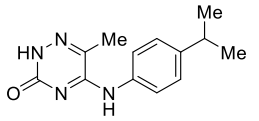	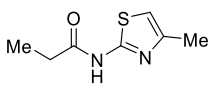	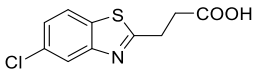	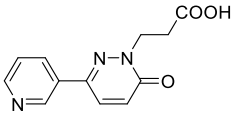
Identification method	High throughput X-ray crystallography	High throughput X-ray crystallography	Virtual screen	Virtual screen
Pocket bound	Ubiquitin	Adjacent	Ubiquitin	Ubiquitin
SPR (K_D, μM)[a]	N.B.[b]	N.B.[b]	60 ± 3	220 ± 20
ITC (K_D, μM)[a]	N.B.[b]	N.B.[b]	40 ± 4	210 ± 30
FP (IC_{50}, μM)[a]	N.I.[c]	N.I.[c]	55 ± 11	350 ± 50
LE[c] (ITC)	-	-	0.40	0.28

[a]Values calculated as average of 3 independent measurements; [b]No Binding; [b]No Inhibition [c]Ligand efficiency was calculated using the equation LE = (1.37 × pK_D)/HA; LE is expressed as kcal mol^{-1} $atom^{-1}$

of HDAC6 Zf-UBD. Together our work comprises a key resource to enable future discovery of potent and selective compounds targeting the HDAC6 Zf-UBD, and probe the functional role of this domain in cells.

RESULTS AND DISCUSSION The structure of HDAC6 Zf-UBD, residues 1109-1215, was previously solved in the apo state (PDB ID: 3C5K) as well as in complex with the RLRGG peptide (PDB ID: 3GV4). The apo structure reveals that this crystal form is not amenable to soaking as the ubiquitin binding pocket is occluded by the C-terminus of the adjacent HDAC6 molecule in the crystal lattice. Using a C-terminally truncated version of this construct, encompassing residues 1109-1213, we found an alternate crystal form, grown using a seed mix of the $HDAC6^{1109-1215}$ crystals. This new crystal form has the same space group and <2.5 % deviation in unit cell dimensions compared to that of the $HDAC6^{1109-1215}$ crystals allowing direct structure solution using the existing 3C5K structure and was also tolerant of 5 % (v/v) DMSO for up to 3 h. The $HDAC6^{1109-1213}$ crystals differ in that residues 1209-1213 are not resolved in the electron density and the ubiquitin binding pocket is not occluded making it accessible to a nearby solvent channel and rendering this crystal form amenable to soaking with small molecules.

Initial ligands of HDAC6 Zf-UBD were identified by two methods (**Table 1**). The new crystal form and soak conditions were used to conduct a high throughput X-ray crystallography fragment screen of 1031 ligands at the LabXChem pipeline based at the i04-1 beamline, Diamond Light Source (U.K.)[42,43], resulting in 571 datasets with 15 map "events" including two fragment hits; **1** which occupies the C-terminal ubiquitin pocket, and **2** which binds in an adjacent pocket. Cocrystal structures of these ligands were solved to 1.07 Å and 1.05 Å resolution for ligands **1** and **2** respectively. In parallel, a virtual screen was conducted using the C-terminal ubiquitin RLRGG peptide bound structure of HDAC6 Zf-UBD (PDB - 3GV4). Cocrystal structures were solved with HDAC6 Zf-UBD in complex with ligands **3** and **4** identified from the virtual screen (**Table 1**) to 1.6 Å and 1.7 Å resolution for ligands **3** and **4** respectively. Both ligands occupy the ubiquitin binding site. For all structures, the position of each non-hydrogen atom of the soaked ligands, pocket residues and water molecules were clear in the electron density permitting precise modelling of the ligand pocket (**Supporting Information**). Together these ligands represent a diverse range of chemotypes.

Two juxtaposed pockets are bound by the ligands

Scheme 1. Synthesis of compounds 8 and 11a-f.[a]

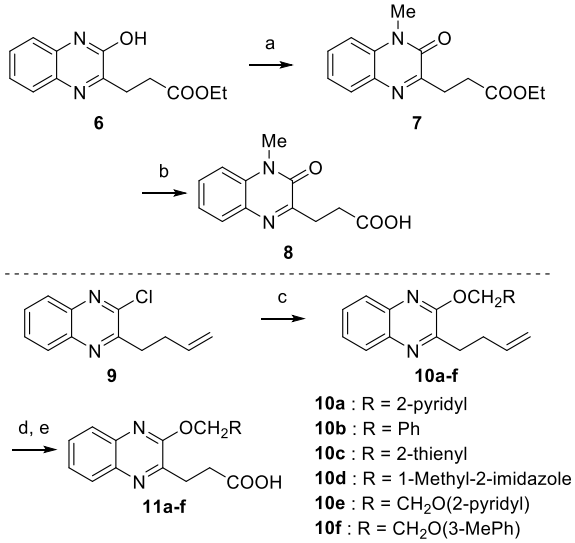

a Reagents and conditions (for synthesis of compounds 6 and 9, see Supporting Information): (a) MeI, K_2CO_3, DMF, rt; (b) LiOH, THF/EtOH/H_2O; (c) ROH, NaH, DMF, rt; (d) Os_4O, $NaIO_4$, THF/ H_2O, 0 °C; (e) $NaClO_2$, NaH_2PO_4, t-BuOH/2-methyl-2-butene, rt.

Table 2. Preliminary SAR ligands by FP assay.

Ligand	Structure	FP calculated IC_{50} (μM)[a]
5	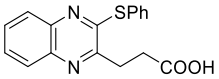	60 ± 9
8	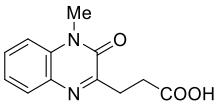	70 ± 10
11a	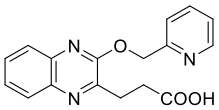	270 ± 80
11b	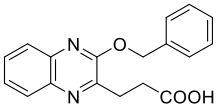	N.B.
11c	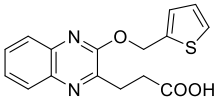	N.B.
11d	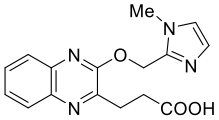	140 ± 60
11e	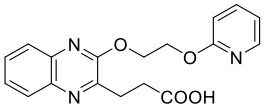	110 ± 40
11f	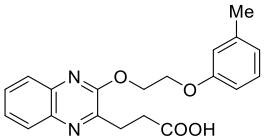	180 ± 40

[a]Average of 3 independent measurements

screened. **3** and **4** both bind in the deep cavity which normally accommodates the C-terminal ubiquitin diglycine motif (**Figure 1D, E**). For both of these compounds the ring groups are stacked between Trp1182 and Arg1155 forming π-stacking and cation-π interactions whilst the carboxylate group occupies the same position as that of the ubiquitin C-terminus. **1** forms the same π-stacking interactions (**Figure 1B**), but lacking the carboxylate group, does not form any interactions deeper in the pocket. A water molecule is found in each cocrystal structure at the end of the ubiquitin binding cavity, coordinating the ligand carboxylate group. **2** binds in a cavity adjacent to the ubiquitin-binding pocket, the thiazole ring stacking on Trp1143 (**Figure 1C**). Interestingly, Arg1155 occupies a similar position to that of the apo structure in this cocrystal, whereas in all ligands involved in π-stacking interactions, this residue swings out to allow efficient stacking of the ring groups between Arg1155 with Trp1182 (**Figure 2A**). By doing so, Arg1155 blocks the channel between the ubiquitin binding pocket and the adjacent pocket. Arg1155 is able to move to accommodate the different ligands as they bind in two distinct pockets, of HDAC6 Zf-UBD, which in turn leads to variability in the shape and connectivity of these two pockets.

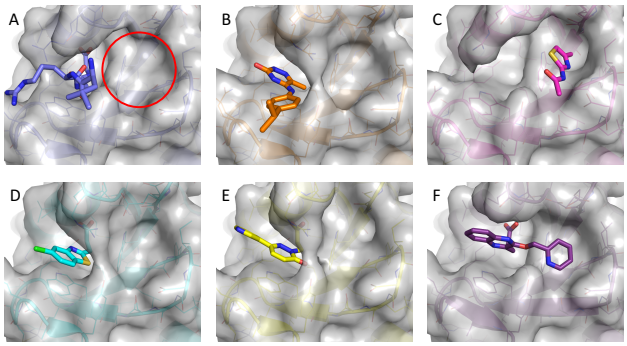

Figure 1: Structures of ligands binding HDAC6 Zf-UBD show the malleability of the pocket. Ubiquitin binding and adjacent pockets shown for HDAC6 Zf-UBD in complex with A) RLRGG with adjacent pocket highlighted with red circle - PDB: 3GV4, B) **1** – PDB: 5KH9, C) **2** - PDB: 5B8D, D) **3** - PDB: 5KH3, E) **4** - PDB: 5KH7 and F) **11b** - PDB: 5PWB.

To characterize HDAC6 Zf-UBD ligand binding *in vitro*, we devised three different biophysical assays (**Figure 3**). Surface plasmon resonance (SPR) and isothermal titration calorimetry (ITC) protocols were optimized to characterize binding kinetics of protein-ligand interactions. To measure direct competition of ligands with ubiquitin, we developed a fluorescence polarization (FP) peptide displacement assay using FITC-labeled RLRGG peptide. K_D values for **3** and **4** were calculated at 60 and 220 μM respectively by SPR (**Table 1**). ITC assay confirmed the K_D values determined by SPR for **3** and **4** (**Table 1**). Similarly, **3** and **4** were able to displace a FITC-labeled RLRGG peptide from $HDAC6^{1109\text{-}1215}$ with IC_{50} values of 55 and 350, respectively. Consistent with the SPR results, these two carboxylate-containing compounds show activity within the μM range and the more potent of the two is **3**. Compound **1** and **2** bind $HDAC6^{1109\text{-}1215}$ but no K_D/IC_{50} values could be determined with any of the three biophysical methods, suggesting that interactions made by the carboxylate group contribute most significantly to potency within this group of ligands.

To explore the potential of improving activity of the fragments, we conducted a preliminary SAR study by testing a limited number of close analogues of the most active hit **3** (**Table 2**). Initially, we tested two commer-

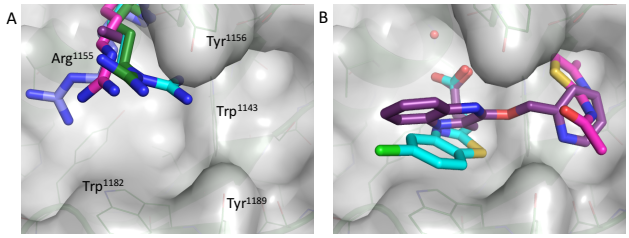

Figure 2: A) Apo HDAC6 - 3C5K (green) modelled with different Arg1155 poses of RLRGG bound - 3GV4 (mauve), 2 bound - 5B8D (magenta), 3 bound - 5KH3 (cyan) and 11b bound - 5PWB (purple). B) Apo HDAC6 - 3C5K (green) is shown with ligands 2 bound - 5B8D (magenta), 3 bound - 5KH3 (cyan) and 11b bound - 5PWB (purple).

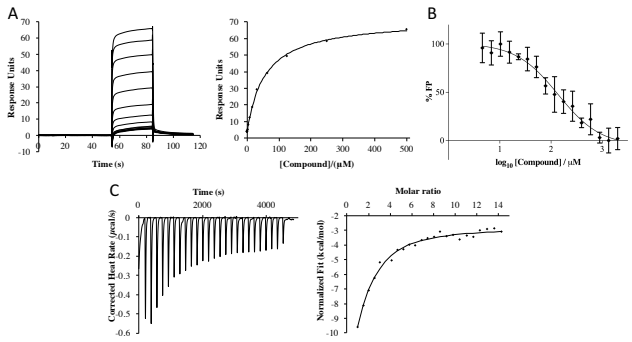

Figure 3: Exemplary assay data of the characterization of ligand **3** by A) SPR, B) ITC and C) FP.

cially available analogues (**5** and **8**) with two different heterocyclic cores, which have the potential of growing into the adjacent pocket with appropriate substitutions at the oxygen or nitrogen atom, by FP assay. Carboxylic acid **8** was resynthesized in house in two steps from the corresponding ethyl ester quinoxaline derivative **6** via regioselective methylation followed by hydrolysis under basic conditions (**Scheme 1**). Both compounds show similar activity to **3**. Our modelling indicated the phenyl group of **5** could potentially reach the adjacent pocket occupied by **2**, but, we could not get a co-crystal structure of **5** with clear ligand electron density to prove this hypothesis.

Encouraged by this result, we synthesized close analogues of **5** with extended linkers to explore the potential of reaching the adjacent pocket with the substitutions at the linker. Compounds **11a-f** were prepared from the chloroquinoxaline derivative **9**. Deprotonation of the desired alcohol with NaH followed by the addition of **9** provided compounds **10a-f**. The tethered double bond functionality was converted into the desired carboxylic acid by Lemieux-Johnson oxidation followed by Pinnick oxidation of the aldehyde intermediate (**Scheme 1**). Compound **11a** showed a moderate drop in activity while the corresponding phenyl analogue **11b** lost activity completely. We were able to co-crystallise HDAC6 Zf-UBD with **11a** and solve the structure to 1.55 Å resolution (PDB – 5PWB). We were delighted to find the pyridyl group occupied the adjacent pocket as predicted (**Figures 1F and 2B**). However, the pi-stacking of the heterocyclic core with Arg1155 and Trp1182 is disrupted. Arg1155 is not fully resolved in the electron density indicating flexibility of this residue in this binding mode, which could explain the weaker affinity of **11a**. We have synthesized analogues of **11a** with two heterocycles (**11c**, **11d**) and analogues with extended linkers (**11e**, **11f**) in order to identify more potent compounds which could pick up additional interactions in the adjacent pocket while maintaining efficient pi stacking in the peptide binding pocket. However, none of the compounds showed improved affinity compared with the original hit. We believe, the activity can be improved by identifying a suitable linker and substitutions, which will allow both heterocyclic ring and substitutions to make optimal interactions in the peptide binding pocket and adjacent pockets respectively.

CONCLUSION We have reported the first small molecules known to bind the HDAC6 Zf-UBD, explored preliminary SAR and identified a compound which can occupy both pockets of this domain. This demonstrates the feasibility of improving the activity of the fragments. We have also reported a robust crystal system to screen ligands by X-ray crystallography and resolve high resolution structures of HDAC6$^{1109\text{-}1213}$ in complex with ligands. Three different biophysical methods (SPR, FP and ITC) were optimized for ligand binding characterisation. The optimized crystal system we developed led to the solution of five high (< 1.7 Å) resolution cocrystal structures of HDAC6$^{1109\text{-}1213}$, revealing the precise binding positions of different compounds with varying affinities (μM to mM). High quality crystallographic data proves especially valuable when modelling the mobile Arg1155 which can block the channel between the ubiquitin and adjacent pockets and such structural details of ligand binding and the subsequent effects on pocket residue positions will be critical if further fragments linking the two pockets are to be designed and characterized to increase the specificity and potency of the inhibitors. HDAC6 Zf-UBD inhibitor development represents a novel approach to dissecting the *in vivo* roles of HDAC6 in both normal cellular function as well as numerous disease states. The optimized assays described in this paper will lay the ground work for forthcoming research to increase the potency of compounds beyond those described in this paper by growing fragments, understanding structure activity relationships and assessing specificity against a panel of other Zf-UBD proteins.

EXPERIMENTAL SECTION

Compounds: All compounds detailed in this paper were assessed for purity using high or ultra-performance liquid chromatography (HPLC/UPLC) and were shown to be >95% purity. 3-(4-methyl-3-oxo-3,4-dihydroquinoxalin-2-yl)propanoic acid (**8**) Step 1: To a mixture of potassium carbonate (68 mg, 0.49 mmol, 1.2 equiv) and **6** (100 mg, 0.41 mmol, 1.0 equiv) in dry DMF (0.2 M) was added MeI (33 μL, 0.53 mmol, 1.3 equiv) and the reaction was stirred at room temperature for 16 h. The resulting mixture was diluted with water and extracted with ethyl acetate. The combined organic layers were dried over $MgSO_4$ and concentrated in vacuo. The crude mixture was purified by flash chromatography (SiO_2, hexanes/ethyl acetate 1:1) to afford 3-(3-oxo-3,4-dihydroquinoxalin-2-yl)propanoic acid (**7**) as an off-white solid (94 mg, 90%). Step 2**.** To a mixture of **7** (50 mg, 0.19 mmol, 1.0 equiv) in a 3:1:1 THF-EtOH-H_2O mixture (0.03 M) was added LiOH·H_2O (18 mg, 0.77 mmol, 4.0 equiv) and the reaction was stirred at room temperature till completion (TLC, 4 h). The resulting mixture was diluted with water and concentrated *in vacuo*. The residue was carefully acidified with aq. HCl 1N to pH 6-7. The resulting solid was filtered, washed with water and dried to afford compound **8** as a white solid (26 mg, 58%).

General Procedure for the Synthesis of Compounds **10a-f.** To a suspension of NaH (1.2 equiv) in DMF (0.2 M) was added the desired alcohol (1.2-2.0 equiv). After 15 minutes stirring at room temperature, a solution of **9** (1.0 equiv) in DMF was added and the reaction was stirred at room temperature till completion (TLC, 2-6 h). The reaction was diluted with ethyl acetate and quenched with sat. aq. NH_4Cl. The aqueous phase was extracted with ethyl acetate, the combined organic layers dried over $MgSO_4$ and concentrated *in vacuo*. The crude mixture was

purified by flash chromatography (SiO_2, hexanes/ethyl acetate) to afford the desired compound **10**.

General Procedure for the Synthesis of Compounds **11a-f.** Step 1) To a solution of **10** (1.0 equiv) and Et_3NBnCl (0.1 equiv) in a 5:3 THF-H_2O mixture (0.1 M), a small grain of OsO_4 was added at 0°C. $NaIO_4$ (3.0 equiv) was added and the reaction vigorously stirred at 0°C till completion (TLC, 1-2 h). The reaction was quenched with sat. aq. Na_2SO_3 and the aqueous phase extracted with ethyl acetate. The combined organic layers were dried over $MgSO_4$ and the solvent evaporated *in vacuo*. The crude mixture was purified by flash chromatography (SiO_2, hexanes/ethyl acetate). Step 2) The aldehyde intermediate (1.0 equiv) was immediately dissolved in a 1:1 *t*-BuOH/2-methyl-2-butene mixture (0.05 M). A freshly prepared aq. solution of $NaClO_2$ (10.0 equiv) and NaH_2PO_4 (5.5 equiv) was added and the reaction vigorously stirred at room temperature overnight. The resulting mixture was diluted with water and the organic solvents were evaporated *in vacuo*. The residue was carefully acidified with aq. HCl 1N to pH 6-7. The resulting solid was filtered, washed with water and dried to afford compound **11**.

Cloning, Protein Expression and Purification: DNAs encoding HDAC6$^{1109\text{-}1213}$ and HDAC6$^{1109\text{-}1215}$ were subcloned into a modified pET28 vector encoding a thrombin cleavable (GenBank EF442785) N-terminal His6-tag (pET28-LIC) and HDAC6$^{1109\text{-}1215}$ was also subcloned into a modified pET28 vector encoding an N-terminal AviTag for *in vivo* biotinylation and a C-terminal His6-tag (p28BIOH-LIC) using a ligation-independent InFusion™ cloning kit (ClonTech) and verified by DNA sequencing. Proteins were over-expressed in BL21 (DE3) Codon Plus RIL *E. coli* (Agilent). Cultures were grown in M9 minimal media supplemented with 50 μM $ZnSO_4$ and also 10 μg/mL biotin for HDAC6$^{1109\text{-}1215}$ p28BIOH-LIC expression. Expression cultures were induced using 0.5 mM IPTG overnight at 15 °C. Proteins were purified using nickel-nitrilotriacetic acid (Ni-NTA) agarose resin (Qiagen) and the tag was removed by thrombin for HDAC6$^{1109\text{-}1213}$ pET28-LIC. Uncleaved proteins and thrombin were removed by another pass with Ni-NTA resin. Proteins were further purified using gel filtration (Superdex 75, GE Healthcare). The final concentrations of purified proteins were 5-10 mg/mL as measured by UV absorbance at 280 nm.

Crystallization: The apo crystal form of HDAC6$^{1109\text{-}1215}$ (PDB ID: 3C5K) was previously reported[4]. These crystals can be used to seed for the soaking amenable crystal form for fragment screening. Diluting 1 μL crystal suspension 1:10,000 with mother liquor and vortexing the sample vigorously yields a seed mix. HDAC6$^{1109\text{-}1213}$ can be crystallized in 2 M Na formate, 0.1 M Na acetate pH 4.6, 5 % ethylene glycol in 5:4:1 3.5 mg/mL protein, mother liquor and seed mix per drop. HDAC6$^{1109\text{-}1213}$ crystals were soaked by adding 5 % (v/v) of a 200 mM or 400 mM DMSO-solubilized stock of compounds **1-4** to the drop for 2 hours prior to mounting and cryo-cooling. Cocrystals of **11a** were grown using the same 5:4:1 ratio seeding protocol with 3.5 mg/mL HDAC6$^{1109\text{-}1213}$ pre-incubated with 5:1 molar ratio of the **11a** ligand to concentrated HDAC6 protein.

Data Collection, Structure Determination and Refinement: X-ray diffraction data for HDAC6$^{1109\text{-}1213}$ cocrystals with **3**, **4** or **11a** were collected at 100K at Rigaku FR-E Superbright home source at a wavelength of 1.54178 Å. HDAC6$^{1109\text{-}1213}$ crystals soaked during LabXChem pipeline were collected at 100K at i04-1, Diamond Light Source (Harwell, U.K.) at a wavelength of 0.92819 Å, hit fragment datasets were identified using a DIMPLE-PANDDA[42] pipeline. All datasets were processed with XDS[44] and Aimless[45]. Models were refined with cycles of COOT[46], for model building and visualization, with REFMAC[47], for restrained refinement and validated with MOLPROBITY[48].

Virtual Screening of Compounds: A diverse chemical library of 1.28 million commercial compounds was docked to HDAC6 (PDB code 3GV4), resulting in the selection of 33 hit candidates, 7 of which were confirmed biochemically. Two follow-up rounds of hit expansion produced **3** and **4**.

Surface Plasmon Resonance (SPR): Studies were performed using a Biacore T200 (GE Health Sciences). Approximately 5000 response units (RU) of biotinylated HDAC6$^{1109\text{-}1215}$ were coupled onto one flow cell of a SA chip as per manufacturer's protocol, and an empty flow cell used for reference subtraction. 2-fold serial dilutions of compounds were prepared in 10 mM HEPES pH 7.4, 150 mM NaCl, 0.005 % (v/v) Tween-20, 1 % (v/v) DMSO. K_D determination experiments were performed using single-cycle kinetics with 30 s contact time, 30 μL/min flow rate at 20 °C. K_D values were calculated using steady state affinity fitting and the Biacore T200 Evaluation software.

Fluorescence Polarisation (FP) RLRGG Peptide Displacement: All experiments were performed in 384-well black polypropylene PCR plates (Axygen) in 10 μL volume. Fluorescence polarization (FP) was measured using a BioTek Synergy 4 (BioTek) at excitation and emission wavelengths were 485 nm and 528 nm, respectively. In each well, 9 μL compound solutions in buffer containing 10 mM HEPES pH 7.4, 150 mM NaCl, 1 % (v/v) DMSO were serially diluted. 1 μL 30 μM HDAC6$^{1109\text{-}1215}$ and 500 nM N-terminally FITC-labelled RLRGG were then added to each well. Following 1 min centrifugation at 250 g, the assay was incubated for 10 min before FP analysis. Previous assay optimization with titration of protein concentration at 50 nM peptide showed these conditions gave ~85 % maximum FP.

Isothermal Titration Calorimetry (ITC): HDAC6$^{1109\text{-}1215}$ was diluted to 50 μM in 10 mM HEPES pH 7.4, 150 mM NaCl, 1 % (v/v) DMSO. All compounds were diluted to 1 mM in the same buffer. All ITC measurements were performed at 25 °C on a Nano ITC (TA Instruments). A total of 25 injections, each of 2 μL, were delivered into a 0.167 mL sample cell at a 180-second interval. The data were analyzed using Nano Analyze software and fitted to a one-site binding model.

ASSOCIATED CONTENT

SUPPORTING INFORMATION

The Supporting Information is available free of charge on the ACS Publications website.

X-ray crystallography data collection and refinement statistics as well as chemical synthesis information can be found in: Supporting_Information.pdf

Authors will release atomic coordinates and experimental data upon article publication.

HDAC6 Cocrystal Structure PDB ID Codes:

1 – 5KH9 **2** – 5B8D **3** – 5KH3 **4** – 5KH7 **11b** – 5WPB

AUTHOR INFORMATION

Corresponding Author

Cheryl H. Arrowsmith: email carrow@uhnresearch.ca

Author Contributions

Experiments were performed by RJH, RF, PC, IF and JKA. All authors contributed to writing the manuscript.

Funding Sources

The SGC is a registered charity (number 1097737) that receives funds from AbbVie, Bayer Pharma AG, Boehringer Ingelheim, Canada Foundation for Innovation, Eshelman Institute for Innovation, Genome Canada through Ontario Genomics Institute, Innovative Medicines Initiative (EU/EFPIA) [ULTRA-DD grant no. 115766], Janssen, Merck

& Co., Novartis Pharma AG, Ontario Ministry of Economic Development and Innovation, Pfizer, São Paulo Research Foundation-FAPESP, Takeda, and the Wellcome Trust. Additional funding from the Collaborative Research and Training Experience grant (Aled Edwards 432008-2013) from the Natural Sciences and Engineering Research Council of Canada.

ACKNOWLEDGMENT

We thank Diamond Light Source for access to beamline i04-1 and the XChem facility that contributed to the results within this manuscript.

ABBREVIATIONS

FP, fluorescence polarization; HDAC, histone deacetylase; ITC, isothermal titration calorimetry; LE, ligand efficiency; SPR, surface plasmon resonance; Zf-UBD, zinc-finger ubiquitin binding domain

REFERENCES

(1) Gregoretti, I. V.; Lee, Y.-M.; Goodson, H. V. Molecular Evolution of the Histone Deacetylase Family: Functional Implications of Phylogenetic Analysis. *J. Mol. Biol.* **2004**, *338* (1), 17–31.

(2) de Ruijter, A. J. M.; van Gennip, A. H.; Caron, H. N.; Kemp, S.; van Kuilenburg, A. B. P. Histone Deacetylases (HDACs): Characterization of the Classical HDAC Family. *Biochem. J.* **2003**, *370* (Pt 3), 737–749.

(3) Kawaguchi, Y.; Kovacs, J. J.; McLaurin, A.; Vance, J. M.; Ito, A.; Yao, T. P. The Deacetylase HDAC6 Regulates Aggresome Formation and Cell Viability in Response to Misfolded Protein Stress. *Cell* **2003**, *115* (6), 727–738.

(4) Ouyang, H.; Ali, Y. O.; Ravichandran, M.; Dong, A.; Qiu, W.; MacKenzie, F.; Dhe-Paganon, S.; Arrowsmith, C. H.; Zhai, R. G. Protein Aggregates Are Recruited to Aggresome by Histone Deacetylase 6 via Unanchored Ubiquitin C Termini. *J. Biol. Chem.* **2012**, *287* (4), 2317–2327.

(5) Hard, R. L.; Liu, J.; Shen, J.; Zhou, P.; Pei, D. HDAC6 and Ubp-M BUZ Domains Recognize Specific C-Terminal Sequences of Proteins. *Biochemistry (Mosc.)* **2010**, *49* (50), 10737–10746.

(6) Seigneurin-Berny, D.; Verdel, A.; Curtet, S.; Lemercier, C.; Garin, J.; Rousseaux, S.; Khochbin, S. Identification of Components of the Murine Histone Deacetylase 6 Complex: Link between Acetylation and Ubiquitination Signaling Pathways. *Mol. Cell. Biol.* **2001**, *21* (23), 8035–8044.

(7) Tran, A. D.-A.; Marmo, T. P.; Salam, A. A.; Che, S.; Finkelstein, E.; Kabarriti, R.; Xenias, H. S.; Mazitschek, R.; Hubbert, C.; Kawaguchi, Y.; Sheetz, M. P.; Yao, T.-P.; Bulinski, J. C. HDAC6 Deacetylation of Tubulin Modulates Dynamics of Cellular Adhesions. *J. Cell Sci.* **2007**, *120* (Pt 8), 1469–1479.

(8) Hubbert, C.; Guardiola, A.; Shao, R.; Kawaguchi, Y.; Ito, A.; Nixon, A.; Yoshida, M.; Wang, X.-F.; Yao, T.-P. HDAC6 Is a Microtubule-Associated Deacetylase. *Nature* **2002**, *417* (6887), 455–458.

(9) Williams, K. A.; Zhang, M.; Xiang, S.; Hu, C.; Wu, J.-Y.; Zhang, S.; Ryan, M.; Cox, A. D.; Der, C. J.; Fang, B.; Koomen, J.; Haura, E.; Bepler, G.; Nicosia, S. V.; Matthias, P.; Wang, C.; Bai, W.; Zhang, X. Extracellular Signal-Regulated Kinase (ERK) Phosphorylates Histone Deacetylase 6 (HDAC6) at Serine 1035 to Stimulate Cell Migration. *J. Biol. Chem.* **2013**, *288* (46), 33156–33170.

(10) Lee, S.-W.; Yang, J.; Kim, S.-Y.; Jeong, H.-K.; Lee, J.; Kim, W. J.; Lee, E. J.; Kim, H.-S. MicroRNA-26a Induced by Hypoxia Targets HDAC6 in Myogenic Differentiation of Embryonic Stem Cells. *Nucleic Acids Res.* **2015**, *43* (4), 2057–2073.

(11) Staszkiewicz, J.; Power, R. A.; Harkins, L. L.; Barnes, C. W.; Strickler, K. L.; Rim, J. S.; Bondioli, K. R.; Eilersten, K. J. Silencing Histone Deacetylase–Specific Isoforms Enhances Expression of Pluripotency Genes in Bovine Fibroblasts. *Cell. Reprogramming* **2013**, *15* (5), 397–404.

(12) Aldana-Masangkay, G. I.; Sakamoto, K. M. The Role of HDAC6 in Cancer. *J. Biomed. Biotechnol.* [Online] **2011**, *2011*, 875824. https://www.hindawi.com/journals/bmri/2011/875824/ (accessed Aug 28, 2017).

(13) Pandey, U. B.; Nie, Z.; Batlevi, Y.; McCray, B. A.; Ritson, G. P.; Nedelsky, N. B.; Schwartz, S. L.; DiProspero, N. A.; Knight, M. A.; Schuldiner, O.; Padmanabhan, R.; Hild, M.; Berry, D. L.; Garza, D.; Hubbert, C. C.; Yao, T.-P.; Baehrecke, E. H.; Taylor, J. P. HDAC6 Rescues Neurodegeneration and Provides an Essential Link between Autophagy and the UPS. *Nature* **2007**, *447* (7146), 859–863.

(14) Ganai, S. A. Small-Molecule Modulation of HDAC6 Activity: The Propitious Therapeutic Strategy to Vanquish Neurodegenerative Disorders. [Online early access]. *Curr. Med. Chem.* **2017**. DOI: 10.2174/0929867324666170209104030 Published Online: Feb 8, 2017. http://www.eurekaselect.com/149943/article (accessed Aug 28, 2017).

(15) Zhang, Y.; Li, N.; Caron, C.; Matthias, G.; Hess, D.; Khochbin, S.; Matthias, P. HDAC-6 Interacts with and Deacetylates Tubulin and Microtubules in Vivo. *EMBO J.* **2003**, *22* (5), 1168–1179.

(16) Zheng, K.; Jiang, Y.; He, Z.; Kitazato, K.; Wang, Y. Cellular Defence or Viral Assist: The Dilemma of HDAC6. *J. Gen. Virol.* **2017**, *98* (3), 322–337.

(17) Matsuyama, A.; Shimazu, T.; Sumida, Y.; Saito, A.; Yoshimatsu, Y.; Seigneurin-Berny, D.; Osada, H.; Komatsu, Y.; Nishino, N.; Khochbin, S.; Horinouchi, S.; Yoshida, M. In Vivo Destabilization of Dynamic Microtubules by HDAC6-Mediated Deacetylation. *EMBO J.* **2002**, *21* (24), 6820–6831.

(18) Kovacs, J. J.; Murphy, P. J. M.; Gaillard, S.; Zhao, X.; Wu, J.-T.; Nicchitta, C. V.; Yoshida, M.; Toft, D. O.; Pratt, W. B.; Yao, T.-P. HDAC6 Regulates Hsp90 Acetylation and Chaperone-Dependent Activation of Glucocorticoid Receptor. *Mol. Cell* **2005**, *18* (5), 601–607.

(19) Zhang, X.; Yuan, Z.; Zhang, Y.; Yong, S.; Salas-Burgos, A.; Koomen, J.; Olashaw, N.; Parsons, J. T.; Yang, X.-J.; Dent, S. R.; Yao, T.-P.; Lane, W. S.; Seto, E. HDAC6 Modulates Cell Motility by Altering the Acetylation Level of Cortactin. *Mol. Cell* **2007**, *27* (2), 197–213.

(20) Zhang, Y.; Kwon, S.; Yamaguchi, T.; Cubizolles, F.; Rousseaux, S.; Kneissel, M.; Cao, C.; Li, N.; Cheng, H.-L.; Chua, K.; Lombard, D.; Mizeracki, A.; Matthias, G.; Alt, F. W.; Khochbin, S.; Matthias, P. Mice Lacking Histone Deacetylase 6 have Hyperacetylated Tubulin but are Viable and Develop Normally. *Mol. Cell. Biol.* **2008**, *28* (5), 1688–1701.

(21) Zhang, L.; Liu, S.; Liu, N.; Zhang, Y.; Liu, M.; Li, D.; Seto, E.; Yao, T.-P.; Shui, W.; Zhou, J. Proteomic Identification and Functional Characterization of MYH9, Hsc70, and DNAJA1 as Novel Substrates of HDAC6 Deacetylase Activity. *Protein Cell* **2015**, *6* (1), 42–54.

(22) Pai, M.-T.; Tzeng, S.-R.; Kovacs, J. J.; Keaton, M. A.; Li, S. S.-C.; Yao, T.-P.; Zhou, P. Solution Structure of the Ubp-M BUZ Domain, a Highly Specific Protein Module that Recognizes the C-Terminal Tail of Free Ubiquitin. *J. Mol. Biol.* **2007**, *370* (2), 290–302.

(23) Hao, R.; Nanduri, P.; Rao, Y.; Panichelli, R. S.; Ito, A.; Yoshida, M.; Yao, T.-P. Proteasomes Activate Aggresome Disassembly and Clearance by Producing Unanchored Ubiquitin Chains. *Mol. Cell* **2013**, *51* (6), 819–828.

(24) Kawaguchi, Y.; Kovacs, J. J.; McLaurin, A.; Vance, J. M.; Ito, A.; Yao, T. P. The Deacetylase HDAC6 Regulates Aggresome Formation and Cell Viability in Response to Misfolded Protein Stress. *Cell* **2003**, *115* (6), 727–738.

(25) Banerjee, I.; Miyake, Y.; Nobs, S. P.; Schneider, C.; Horvath, P.; Kopf, M.; Matthias, P.; Helenius, A.; Yamauchi, Y. Influenza A Virus Uses the Aggresome Processing Machinery for Host Cell Entry. *Science* **2014**, *346* (6208), 473–477.
(26) Rudnicka, A.; Yamauchi, Y. Ubiquitin in Influenza Virus Entry and Innate Immunity. *Viruses* [Online] **2016**, *8* (10) http://www. mdpi.com/1999-4915/8/10/293 (accessed Aug 28, 2017).
(27) Lombardi, P. M.; Cole, K. E.; Dowling, D. P.; Christianson, D. W. Structure, Mechanism, and Inhibition of Histone Deacetylases and Related Metalloenzymes. *Curr. Opin. Struct. Biol.* **2011**, *21* (6), 735–743.
(28) Mottamal, M.; Zheng, S.; Huang, T. L.; Wang, G. Histone Deacetylase Inhibitors in Clinical Studies as Templates for New Anticancer Agents. *Mol. Basel Switz.* **2015**, *20* (3), 3898–3941.
(29) Wagner, J. M.; Hackanson, B.; Lübbert, M.; Jung, M. Histone Deacetylase (HDAC) Inhibitors in Recent Clinical Trials for Cancer Therapy. *Clin. Epigenetics* **2010**, *1* (3–4), 117–136.
(30) Miyake, Y.; Keusch, J. J.; Wang, L.; Saito, M.; Hess, D.; Wang, X.; Melancon, B. J.; Helquist, P.; Gut, H.; Matthias, P. Structural Insights into HDAC6 Tubulin Deacetylation and Its Selective Inhibition. *Nat. Chem. Biol.* **2016**, *12* (9), 748–754.
(31) Hideshima, T.; Bradner, J. E.; Wong, J.; Chauhan, D.; Richardson, P.; Schreiber, S. L.; Anderson, K. C. Small-Molecule Inhibition of Proteasome and Aggresome Function Induces Synergistic Antitumor Activity in Multiple Myeloma. *Proc. Natl. Acad. Sci. U. S. A.* **2005**, *102* (24), 8567–8572.
(32) Amengual, J. E.; Johannet, P.; Lombardo, M.; Zullo, K.; Hoehn, D.; Bhagat, G.; Scotto, L.; Jirau-Serrano, X.; Radeski, D.; Heinen, J.; Jiang, H.; Cremers, S.; Zhang, Y.; Jones, S.; O'Connor, O. A. Dual Targeting of Protein Degradation Pathways with the Selective HDAC6 Inhibitor ACY-1215 and Bortezomib Is Synergistic in Lymphoma. *Clin. Cancer Res. Off. J. Am. Assoc. Cancer Res.* **2015**, *21* (20), 4663–4675.
(33) Santo, L.; Hideshima, T.; Kung, A. L.; Tseng, J.-C.; Tamang, D.; Yang, M.; Jarpe, M.; van Duzer, J. H.; Mazitschek, R.; Ogier, W. C.; Cirstea, D.; Rodig, S.; Eda, H.; Scullen, T.; Canavese, M.; Bradner, J.; Anderson, K. C.; Jones, S. S.; Raje, N. Preclinical Activity, Pharmacodynamic, and Pharmacokinetic Properties of a Selective HDAC6 Inhibitor, ACY-1215, in Combination with Bortezomib in Multiple Myeloma. *Blood* **2012**, *119* (11), 2579–2589.
(34) Vogl, D. T.; Raje, N. S.; Jagannath, S.; Richardson, P. G.; Hari, P.; Orlowski, R. Z.; Supko, J. G.; Tamang, D.; Yang, M.; Jones, S. S.; Wheeler, C.; Markelewicz, R. J.; Lonial, S. Ricolinostat, the First Selective Histone Deacetylase 6 Inhibitor, in Combination with Bortezomib and Dexamethasone for Relapsed or Refractory Multiple Myeloma. *Clin. Cancer Res. Off. J. Am. Assoc. Cancer Res.* **2017**, *23* (13), 3307-3315
(35) Simms-Waldrip, T.; Rodriguez-Gonzalez, A.; Lin, T.; Ikeda, A. K.; Fu, C.; Sakamoto, K. M. Targeting the Aggresome Pathway in Hematologic Malignancies. *Mol. Genet. Metab.* **2008**, *94* (3), 283–286.
(36) Hideshima, T.; Qi, J.; Paranal, R. M.; Tang, W.; Greenberg, E.; West, N.; Colling, M. E.; Estiu, G.; Mazitschek, R.; Perry, J. A.; Ohguchi, H.; Cottini, F.; Mimura, N.; Görgün, G.; Tai, Y.-T.; Richardson, P. G.; Carrasco, R. D.; Wiest, O.; Schreiber, S. L.; Anderson, K. C.; Bradner, J. E. Discovery of Selective Small-Molecule HDAC6 Inhibitor for Overcoming Proteasome Inhibitor Resistance in Multiple Myeloma. *Proc. Natl. Acad. Sci. U. S. A.* **2016**, *113* (46), 13162–13167.
(37) Butler, K. V.; Kalin, J.; Brochier, C.; Vistoli, G.; Langley, B.; Kozikowski, A. P. Rational Design and Simple Chemistry Yield a Superior, Neuroprotective HDAC6 Inhibitor, Tubastatin A. *J. Am. Chem. Soc.* **2010**, *132* (31), 10842–10846.
(38) Haggarty, S. J.; Koeller, K. M.; Wong, J. C.; Grozinger, C. M.; Schreiber, S. L. Domain-Selective Small-Molecule Inhibitor of Histone Deacetylase 6 (HDAC6)-Mediated Tubulin Deacetylation. *Proc. Natl. Acad. Sci. U. S. A.* **2003**, *100* (8), 4389–4394.
(39) Jochems, J.; Boulden, J.; Lee, B. G.; Blendy, J. A.; Jarpe, M.; Mazitschek, R.; Van Duzer, J. H.; Jones, S.; Berton, O. Antidepressant-Like Properties of Novel HDAC6-Selective Inhibitors with Improved Brain Bioavailability. *Neuropsychopharmacology* **2014**, *39* (2), 389–400.
(40) Suzuki, T.; Miyata, N. Non-Hydroxamate Histone Deacetylase Inhibitors. *Curr. Med. Chem.* **2005**, *12* (24), 2867–2880.
(41) Giannini, G.; Cabri, W.; Fattorusso, C.; Rodriquez, M. Histone Deacetylase Inhibitors in the Treatment of Cancer: Overview and Perspectives. *Future Med. Chem.* **2012**, *4* (11), 1439–1460.
(42) Pearce, N. M.; Bradley, A. R.; Krojer, T.; Marsden, B. D.; Deane, C. M.; von Delft, F. Partial-Occupancy Binders Identified by the Pan-Dataset Density Analysis Method Offer New Chemical Opportunities and Reveal Cryptic Binding Sites. *Struct. Dyn. Melville N* **2017**, *4* (3), 32104.
(43) Pearce, N. M.; Krojer, T.; Bradley, A. R.; Collins, P.; Nowak, R. P.; Talon, R.; Marsden, B. D.; Kelm, S.; Shi, J.; Deane, C. M.; von Delft, F. A Multi-Crystal Method for Extracting Obscured Crystallographic States from Conventionally Uninterpretable Electron Density. *Nat. Commun.* **2017**, *8*, 15123.
(44) Kabsch, W. XDS. *Acta Crystallogr. D Biol. Crystallogr.* **2010**, *66*, 125–132.
(45) Evans, P. R.; Murshudov, G. N. How Good Are My Data and What Is the Resolution? *Acta Crystallogr. D Biol. Crystallogr.* **2013**, *69*, 1204–1214.
(46) Emsley, P.; Lohkamp, B.; Scott, W. G.; Cowtan, K. Features and Development of Coot. *Acta Crystallogr. D Biol. Crystallogr.* **2010**, *66*, 486–501.
(47) Murshudov, G. N.; Skubák, P.; Lebedev, A. A.; Pannu, N. S.; Steiner, R. A.; Nicholls, R. A.; Winn, M. D.; Long, F.; Vagin, A. A. REFMAC5 for the Refinement of Macromolecular Crystal Structures. *Acta Crystallogr. D Biol. Crystallogr.* **2011**, *67*, 355–367.
(48) Chen, V. B.; Arendall, W. B.; Headd, J. J.; Keedy, D. A.; Immormino, R. M.; Kapral, G. J.; Murray, L. W.; Richardson, J. S.; Richardson, D. C. MolProbity: All-Atom Structure Validation for Macromolecular Crystallography. *Acta Crystallogr. D Biol. Crystallogr.* **2010**, *66*, 12–21.

TOC Graphic:

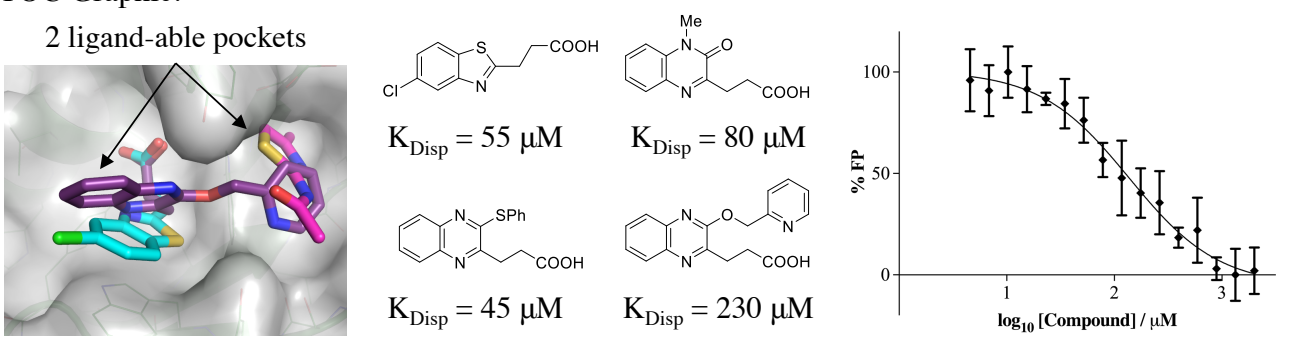

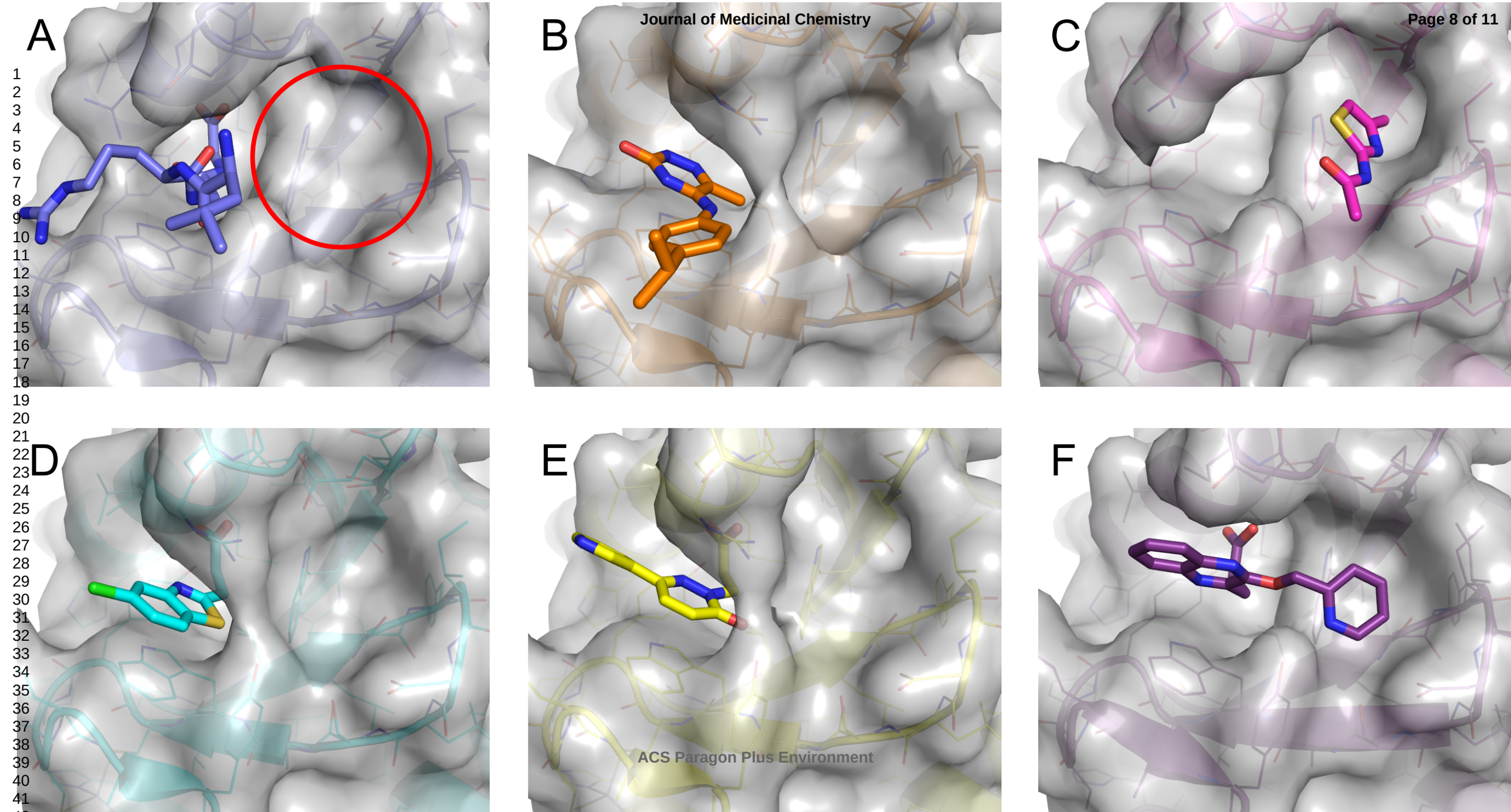
A
B
C
D
E
F
ACS Paragon Plus Environment

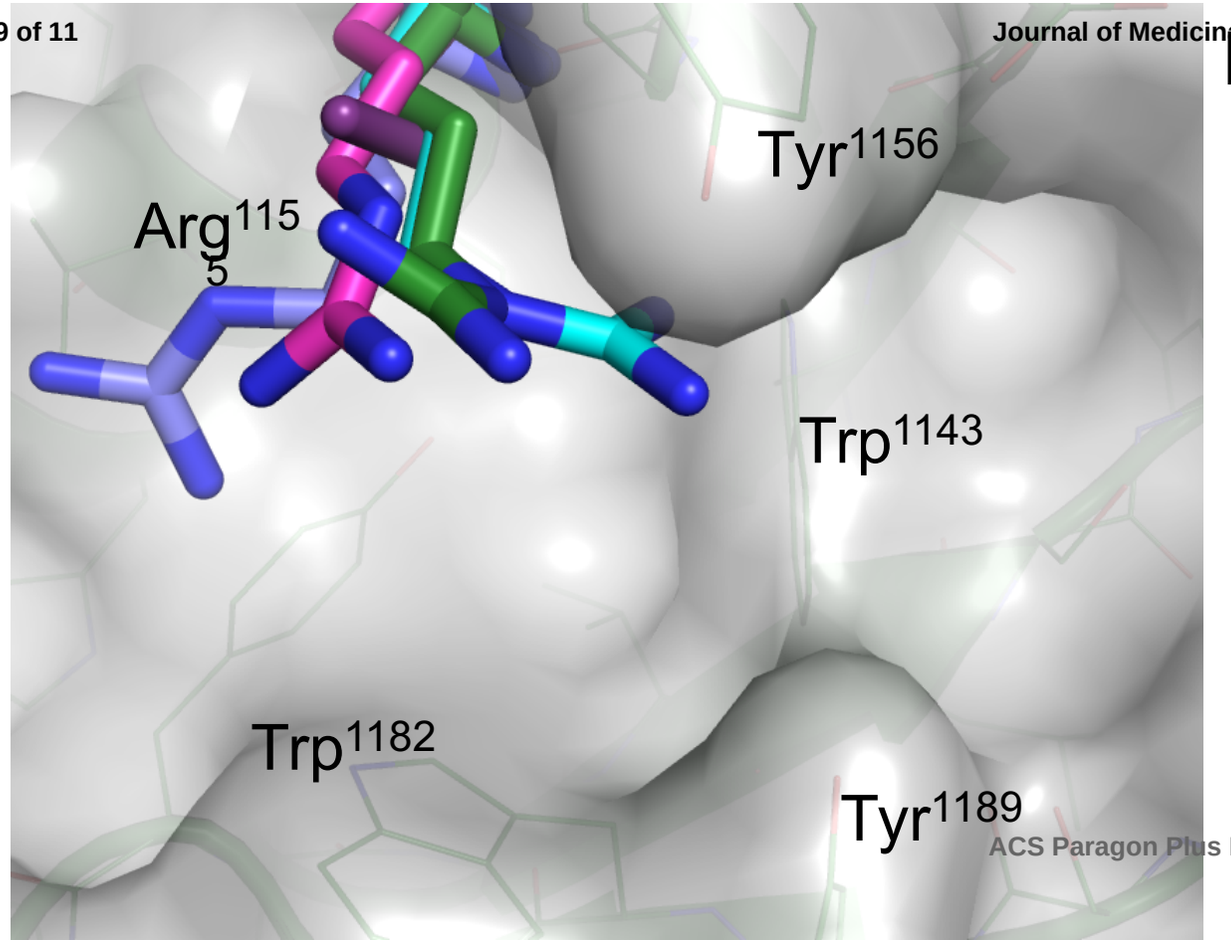

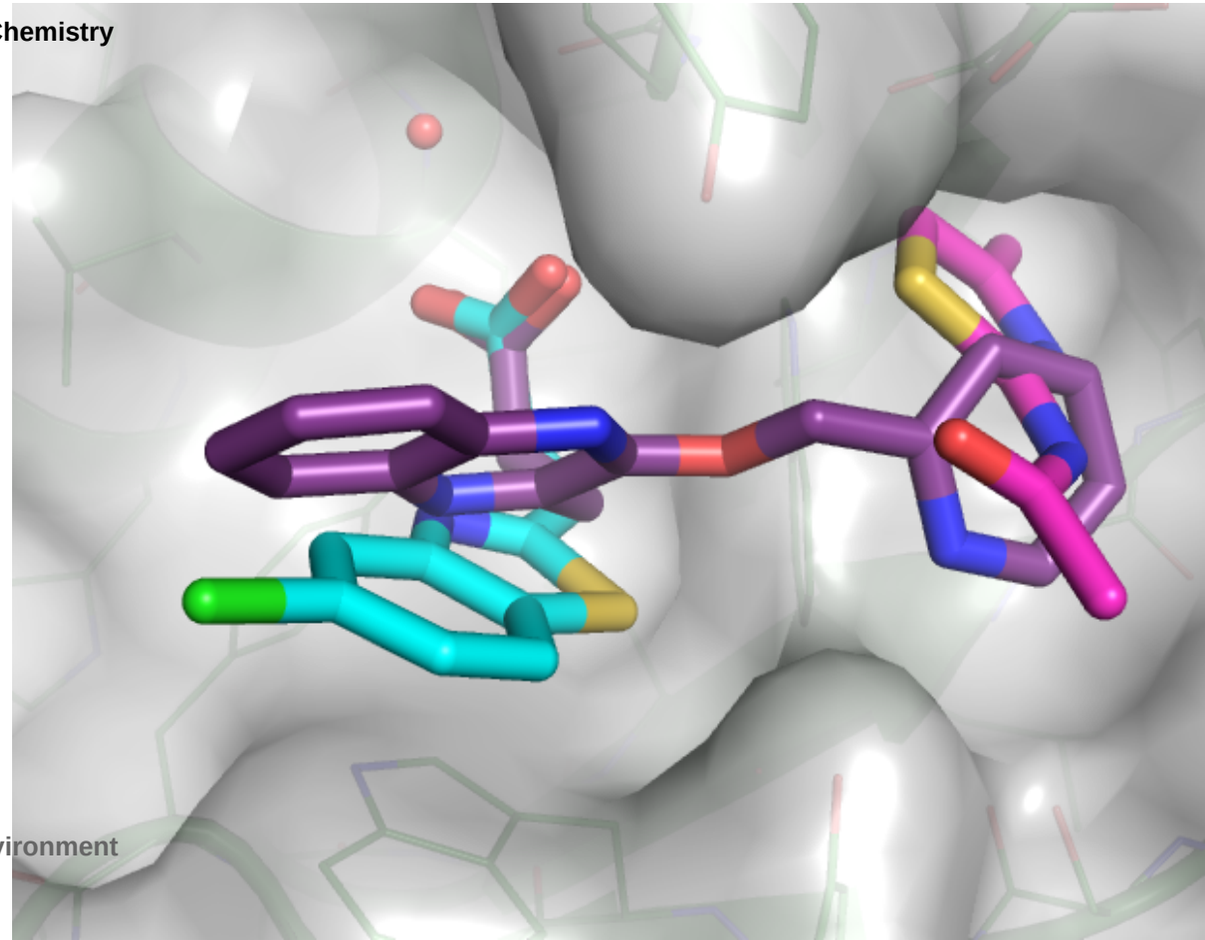

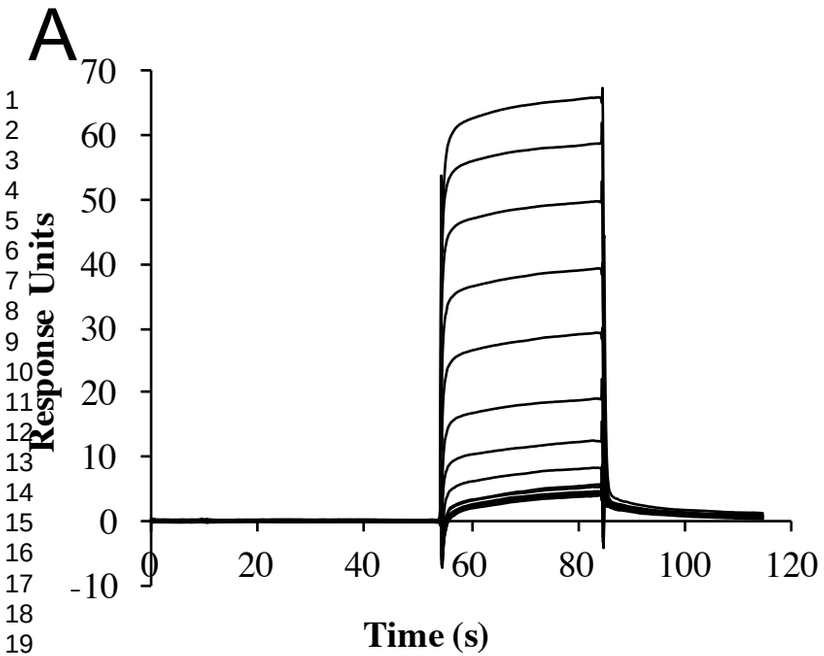

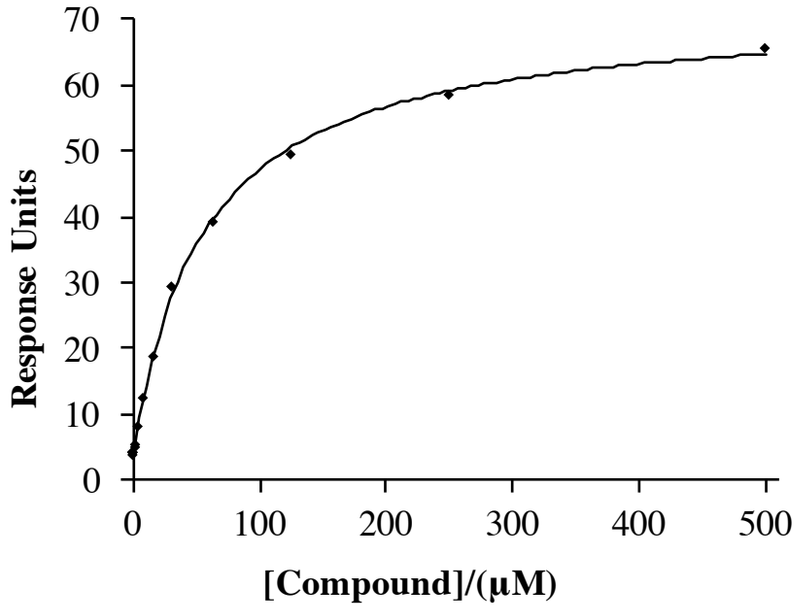

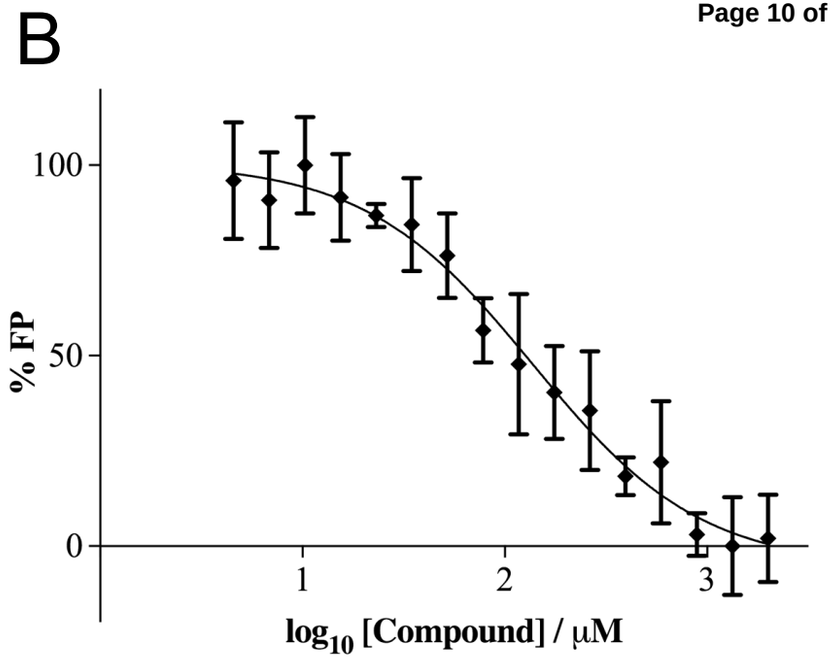

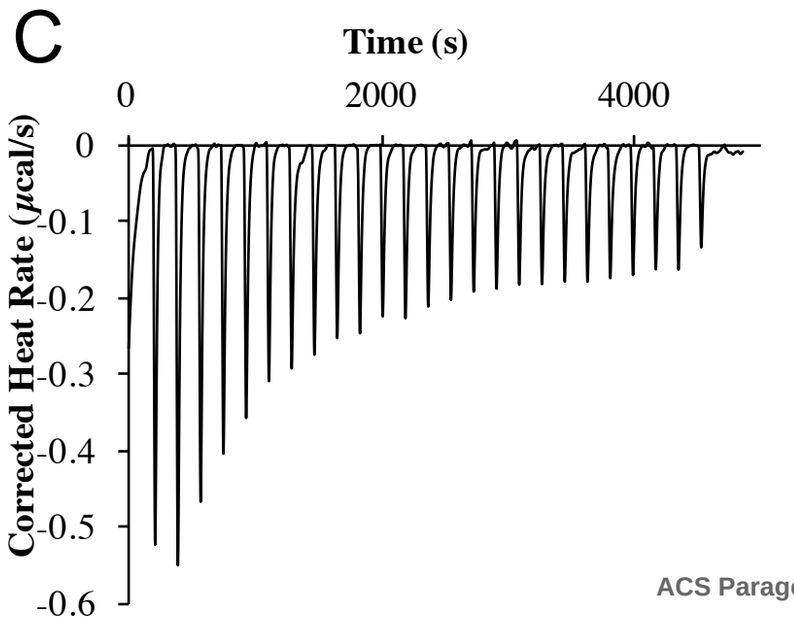

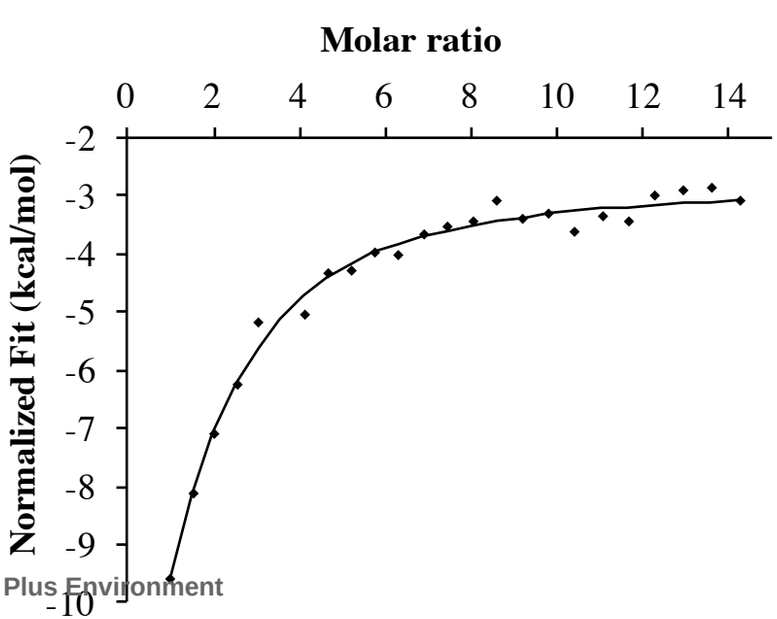

2 ligand-able pockets

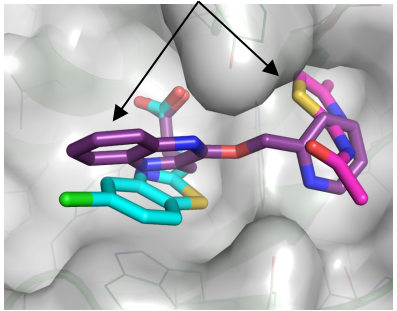

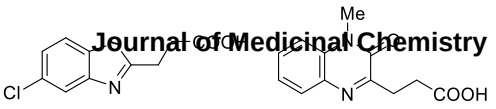

K_{Disp} = 55 μM

K_{Disp} = 80 μM

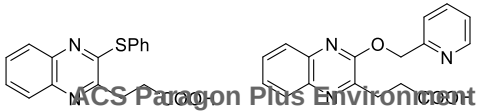

K_{Disp} = 45 μM

K_{Disp} = 230 μM